



CHORUS

This is the accepted manuscript made available via CHORUS. The article has been published as:

Fermi surface of the flat-band intermetallics $APd_{\{3\}}$ ($A=Pb,Sn$)

Kaya Wei, Kuan-Wen Chen, Jennifer N. Neu, You Lai, Greta L. Chappell, George S. Nolas,
David E. Graf, Yan Xin, Luis Balicas, Ryan E. Baumbach, and Theo Siegrist

Phys. Rev. Materials **3**, 041201 — Published 3 April 2019

DOI: [10.1103/PhysRevMaterials.3.041201](https://doi.org/10.1103/PhysRevMaterials.3.041201)

Fermi Surface of the Flat-Band Intermetallics APd_3 ($A = Pb, Sn$)

Kaya Wei,^{1,‡,*} Kuan-Wen Chen,^{1,2,‡} Jennifer N. Neu,^{1,2} You Lai,^{1,2} Greta L. Chappell,^{1,2} George S. Nolas,³ David E. Graf,¹ Yan Xin,¹ Luis Balicas,^{1,2} Ryan E. Baumbach,^{1,2} and Theo Siegrist^{1,4}

¹*National High Magnetic Field Laboratory, Florida State University, Tallahassee, Florida 32310, USA*

²*Department of Physics, Florida State University, Tallahassee, Florida 32306, USA*

³*Department of Physics, University of South Florida, Tampa, Florida 33620, USA*

⁴*Department of Chemical and Biomedical Engineering, FAMU-FSU College of Engineering, Tallahassee, Florida 32310, USA*

Abstract

The intermetallic phases APd_3 ($A = Pb, Sn$) were recently predicted to host an unconventional combination of novel electronic structure features, namely flat bands near the Fermi energy coexisting with topologically protected surface states at the Γ point. These features each could independently produce novel electronic states, including electronically or magnetically ordered states coexisting with unconventional edge dominated transport and a significantly large thermopower coexisting with topological characteristics. To investigate these expectations, we report the synthesis, structural/chemical characterization, electrical and thermal transport properties, magnetic torque (up to 45 T), and Fermi surface mapping for single crystals produced using the Czochralski technique. X-ray diffraction and scanning transmission electron microscope measurements establish the absence of defects, while small measured values of the thermopower indicate that the Fermi level is located away from the flat band region. The electronic properties are further clarified by the topography of the Fermi surfaces, measured through the de Haas–van Alphen effect. We find that the Fermi levels are placed at higher energy values than the original ones resulting from the density functional theory calculations, 54 meV higher for $PbPd_3$ and 68 meV higher for $SnPd_3$. The molten flux method was also used to synthesize $PbPd_3$, yielding nearly identical Fermi surfaces between the specimens grown using different synthesis techniques, indicating the robustness of the Fermi level position. According to the density functional theory calculations, the flat band is mainly formed by the $4d$ bands of Pd. Therefore, we propose monovalent doping on the Pb/Sn site as a viable approach to accessing the flat band while maintaining the unique band structure features of these compounds.

[‡] K. Wei and K.-W. Chen contributed equally.

* Corresponding author.

In recent years there have been far reaching efforts to search for three-dimensional topological semimetals, which offer a chance to explore topological matters through an approach that is separate from topological insulators. Amongst these materials, the compounds APd_3 ($A = Pb, Sn$) were identified as candidate-materials where the density functional theory (DFT) based methods reveal: (i) a dispersionless band along the Γ -X line lying closely to the Fermi level (E_F); (ii) triple nodal points and three-dimensional nodal loops in the absence of spin-orbit coupling (SOC); (iii) Fermi arcs and Dirac surface states presenting clearly within the Perdew-Burke-Ernzerhof generalized gradient approximation (GGA)+SOC; and (iv) topological characteristics on the $k_z = 0$ plane [1]. Exotic physical properties are expected due to these fascinating features. For instance, the unconventional surface state might enable topological protection, making these compounds potential candidates for applications involving topological matter [2-4]. In addition, the large electronic density of states (DOS) of the flat band may promote novel bulk electronic properties such as an enhanced Seebeck coefficient (thermopower) or superconductivity [5-10]. A very recent study also suggests a large transverse magnetoresistance in $PbPd_3$, 650% at 1.8 K under 14 T [11].

In this study, we synthesized large single crystals of $PbPd_3$ and $SnPd_3$ by the Czochralski technique. The crystal structure and $Pb(Sn) - Pd$ site ordering were characterized using both X-ray diffraction (XRD) and scanning transmission electron microscopy (STEM) which reveal negligible chemical or site disorder. The thermoelectric properties and magnetic torque (up to 45 T) were measured for both compounds. The geometry of the Fermi surfaces was revealed through the de Haas-van Alphen (dHvA) effect which was detected in the magnetic torque. In order to further verify these results, $PbPd_3$ was also synthesized using a Pb flux method, where we find the angular dependence of the dHvA oscillations to be nearly identical to that of the samples grown using the Czochralski process. By comparison with the DFT calculations, we conclude that the Fermi surface features revealed by dHvA oscillations indicate the E_F to be placed at higher energies than the values calculated by DFT [1]: $\Delta E_F = 54$ meV and 68 meV for $PbPd_3$ and $SnPd_3$, respectively. This result is supported by the small Seebeck coefficient values which indicate that the E_F is displaced away from the flat band. We propose strategies to tune E_F with a focus on maintaining the flat band feature while placing E_F near the surface state or the bulk state.

Single crystals of APd_3 were obtained through Czochralski process (Figs.1 (a) and 1 (b)). During both growths, the melts were prepared by melting the pure elements using induction heating in W crucibles in a ratio of $A:Pd = 1:3$ and pulling at a speed of 5 mm/h under 1200 °C and 1350 °C for $PbPd_3$ and $SnPd_3$, respectively. The as-synthesized crystals were sealed under vacuum in quartz tubes and annealed at 800 °C and 950 °C for $PbPd_3$ and $SnPd_3$, respectively, for 30 days to release any strain formed during the Czochralski process and ensure $Pb(Sn) - Pd$ order. A molten Pb flux was also used to synthesize $PbPd_3$ single crystals. Elemental Pb and Pd were loaded into a 2-mL alumina crucible with the ratio of $Pb:Pd = 1:20$ and sealed under vacuum within a quartz tube. These mixtures were heated at a rate of 50 °C/h to 1100 °C, held at this temperature for 1

day and slowly cooled at a rate of 2 °C/h to 500 °C. The obtained crystals were subsequently centrifuged to separate them from the molten Pb flux. A Scintag PAD-V Theta/2-Theta reflection powder diffractometer (with line focus CuK α beam and graphite analyzer together with a scintillator detector) and a custom-built diffractometer system (Rigaku rotating anode CuK α source, graphite monochromatized in non-dispersive geometry for high signal/noise ratio) were used to check the crystal structure, phase purity and site ordering of the crystals.

Samples were prepared for TEM measurements by crushing the crystals in ethanol with a mortar and pestle. The suspension of crushed crystals was then dropped onto a 200 μm mesh carbon/formvar film TEM copper grid with a pipette. Sample prepared this way preserved the pristine and original quality of the crystals. The high-angle-annular-dark-field STEM (HAADF-STEM) study was carried out using a probe-aberration-corrected, cold field-emission JEM JEOL-ARM200cF at 200 kV using a JEOL HAADF-STEM detector. The STEM imaging resolution is 0.078 nm. HAADF-STEM images were acquired using 30 μm condenser lens aperture, at a camera length of 8 cm corresponding to a collection angle of 58.7 mrad, and an image scan speed of 32 $\mu\text{s}/\text{pixel}$. The beam convergent angle was 21 mrad.

Single crystals of APd₃ were aligned using an Enraf-Nonius CAD-4 diffractometer along their [100]-axis before being cut into a rectangular slab of 2 mm \times 2 mm \times 5 mm dimensions for temperature dependent four-probe electrical resistivity ρ , Seebeck coefficient S (gradient sweep method), and steady-state thermal conductivity κ measurements in the temperature range from 12 to 300 K. The crystals were mounted such that the current and the thermal gradient were both applied along the [100] direction. All the surfaces were polished using 3 μm grit diamond polishing paper to reduce surface radiation losses during the measurements. The measurements were performed in a custom radiation-shielded vacuum probe with uncertainties of 4, 6, and 8% for ρ , S , and κ measurements, respectively [12]. Electrical contacts to the specimens were made using silver epoxy and thermal contacts were made using Stycast epoxy. The magnetic torque τ was measured using a piezoelectric cantilever (SEIKO-PRC400) in the 45 T hybrid magnet at the National High Magnetic Field Laboratory in Tallahassee.

DFT calculations were performed using the Wien2K [13] implementation. We used the full-potential linearized augmented plane-wave method with the Perdew-Burke-Ernzerhof parametrization of the generalized gradient approximation (GGA-PBE) [14]. The Brillouin zone was sampled by a dense k mesh $40 \times 40 \times 40$ and the basis set cutoff $R_{\text{mt}}K_{\text{max}} = 9$, following the same condition as in [1]. SOC was included in all of our calculations. The angular dependency of the oscillatory frequencies associated with each Fermi-surface cross-sectional area were computed through defining Supercell K-space Extremal Area Finder (SKEAF) code [15].

The as-synthesized crystals are shown in Figs. 1(a)-(c). The Czochralski technique yields single crystals with 23-25 mm in length. After annealing, the surface of the Czochralski-grown crystals began to show faceting parallel to the pulling direction and around the quasi-cylindrical body of the crystals. For the flux-grown PbPd_3 , cubic shape crystals with well-defined surfaces were obtained after removing the flux through centrifuging at elevated temperatures. We checked multiple Czochralski-grown crystals using STEM and did not observe disorder at the atomic resolution levels of the microscope (Figs. 1(d) and 1(e)). Energy dispersive spectroscopy (EDS) confirmed that the stoichiometry was uniformly 1:3 in APd_3 . In another approach to rule out the presence of disorders/vacancies in the specimens, we ground the crystals into fine powder and analyzed the powder XRD patterns with a focus on the A -Pd site occupancy preference (Fig. 2). We confirmed that indeed all of our samples crystallized in the cubic Cu_3Au -type structure ($Pm\bar{3}m$, space group # 221, $a = 4.0357(8)$ and $3.9759(7)$ for PbPd_3 and SnPd_3 , respectively) with full preferred site occupancy. The fact that the (100), (110), and (210) reflections are clearly observed is strong evidence of site ordering since the mixed site occupancy leads to an apparent higher symmetry structure ($Fm\bar{3}m$, space group # 225) with the reflections listed above as unobserved. Furthermore, using these reflections we estimate the ordering parameters to be close to 1 for the Czochralski-grown SnPd_3 , the Czochralski-grown PbPd_3 , and the flux-grown PbPd_3 . We note that the magnetic torque and the transport properties measurements that will be described below were performed on the crystals grown through the Czochralski process.

DFT calculations predict that the E_F is located at the flat band. This leads to the expectation that there should be a significant derivative $dN(E)/dE$ in the DOS at E_F . As a result, the Seebeck coefficient is expected to show a large value, making these materials interesting for thermoelectric applications. We therefore investigated the thermoelectric properties of APd_3 (Fig. 3 and Fig. S1). Fig. 3(a) shows κ and the lattice contribution to κ (κ_L) of APd_3 from 12 K to 300 K. Employing the Wiedemann–Franz relation, the electronic thermal conductivity, κ_E , can be estimated from the relationship $\kappa_E = L_0\sigma T$ with the Lorenz number, $L_0 = 2.45 \times 10^{-8} \text{ V}^2\text{K}^{-2}$ [16]. Thus, κ_L can be estimated from $\kappa - \kappa_E$. At low temperatures, the phonon mean free path is limited by grain boundaries, which in this case corresponds to the size of the measured single crystal. The solid lines in Fig. 3(a) represent the T^3 temperature dependence of κ_L which agree well with the measured data, indicating predominant boundary scattering of phonons [16]. $S(T)$ for APd_3 are shown in Fig. 3(b). As the temperature decreases, the Seebeck coefficients of both PbPd_3 and SnPd_3 decrease accordingly. The Seebeck coefficient of SnPd_3 changes from positive to negative around 160 K, and the curvatures in the $S(T)$ data indicate the competition between electrons and holes at the E_F . This corroborates the previously projected Fermi surface [1] and our Fermi surface mapping (to be discussed later) in which both electron- and hole-pockets were observed. The absolute values of the Seebeck coefficient, on the other hand, suggest that the E_F is placed away from the flat band. In fact, while the predicted E_F of PbPd_3 lies near the flat band, by varying the electron concentration through Bi-doping on the Pb site, the E_F , as well as the corresponding Seebeck coefficient, of $(\text{Pb}_{1-x}\text{Bi}_x)\text{Pd}_3$ were calculated for $x = 0.01, 0.02, 0.03,$ and 0.033 [1]. We note that our measured Seebeck coefficient would be equivalent to that of the 3% doping which corresponds to an E_F about 54 meV higher than the DFT prediction. We

plotted the calculated Seebeck coefficient of 3% Bi-doped PbPd₃ together with our measured data as a comparison (dash-dot line in Fig. 3(b)).

Fig. 4 shows the electronic band structures of APd₃. Based on our DFT calculations and previously reported results [1], a dispersionless flat band exists along the Γ -X direction for both compounds. The band gaps of the bulk states at the Γ point are about 0.4 eV for PbPd₃ and 0.1 eV for SnPd₃. Together with the observed nontrivial surface states, our results agree with these predictions in Ref. [1]. Furthermore, for both PbPd₃ and SnPd₃, there are ellipsoidal shaped hole pockets (α pockets) along Γ -R and a large, nearly spherical electron pockets near the R point, as shown in Figs. 5(a) and 5(b). The cubic β hole-pocket near the Γ point, however, only appears in PbPd₃. We attribute this to the fact that the E_F of SnPd₃ is located within the gap at the Γ point. While the E_F is calculated directly from DFT, which is consistent with reference [1], E_F is the shifted Fermi level based on the experimental quantum oscillations data (discussed below). We note that both E_F s measured by our dHvA oscillations are higher than those predicted from previous DFT calculations; $\Delta E_F = 54$ meV and 68 meV for PbPd₃ and SnPd₃, respectively. The differences are within the error bars inherent to DFT which is often seen in studies involving both DFT calculations and experimental approaches in terms of band structure determination. While it is generally acknowledged that uncertainties exist in exactly pinpointing the E_F using different implementations of DFT, our E_F for PbPd₃, as revealed from the dHvA oscillations, along with the measured Seebeck coefficient values appear to be equivalent to that of the 3% Bi-doped PbPd₃ in Ref. [1].

Torque magnetometry measurements are ideal to construct the Fermi surface via the dHvA effect. Due to an external magnetic field $\mu_0 H$, the cyclotron orbit becomes quantized and with increasing the field the separation in energy between Landau levels rise accordingly. Therefore, DOS is modulated periodically as a function of the inverse of the induction field B as the Landau levels cross and leave the chemical potential, according to the Lifshitz-Onsager quantization rule,

$$\frac{1}{B_n} = \frac{2\pi e}{\hbar} [n + \gamma] \frac{1}{A}, (n = 0, 1, 2 \dots)$$

where A is the extremal cross-sectional area of the Fermi surface normal to B , e is the electron charge, \hbar is Planck constant and γ is the Onsager phase. The oscillatory dHvA signal was isolated by subtracting a smooth polynomial background from $\tau(B)$. The frequencies F were then identified by using a fast Fourier transform (Figs. 5(c) and 5(d)). The topography of the Fermi surface revealed by the quantum oscillations is consistent with the DFT calculations, where there are three nearly isotropic pockets labeled α , β , and γ . We extracted the quantum oscillation frequencies of $F_\alpha = 110$ T, $F_\beta = 180$ T, and $F_\gamma = 1650$ T at an angle θ (between the principle axis, while rotating from [100] to [110], and B) = 25°. We point out that the DFT calculations overestimate the size of the γ pocket while underestimating the size of the α pocket in PbPd₃ (Fig. 5(c)). A close inspection revealing low frequencies for the flux-grown specimen are shown in the Supporting Information (Fig. S2) [17]. For SnPd₃, we extracted $F_\alpha = 170$ T and $F_\gamma = 2500$ T at θ

= 30°. In this case the DFT calculations agree well with the experimental results in both the size and topography of the Fermi surfaces (Fig. 5(d)).

According to the Lifshitz-Kosevich (LK) formula [18], the temperature and the field dependencies of the oscillation amplitudes are described by the product of the thermal damping factor, $R_T = \alpha T m^* / B \sinh(\alpha T m^* / B)$ and the Dingle damping factor $R_D = \exp(-\alpha T_D m^* / B)$, where m^* is the quasiparticle effective mass and T_D is the Dingle temperature ($T_D = \hbar / 2\pi k_B \tau_s$). One can further evaluate the scattering time τ_s and $\alpha = 2\pi^2 k_B m_e / e \hbar \approx 14.69$ T/K with a carrier mobility $\mu_q = e\tau q / m^*$. By fitting the amplitude of the FFT peaks as a function of the temperature to the thermal damping factor, we extracted the carrier effective masses m^* , as shown in Fig. 6. Specifically, we obtained $m_{\alpha}^* = 0.12 m_0$, $m_{\beta}^* = 0.09 m_0$, and $m_{\gamma}^* = 0.38 m_0$ for PbPd₃, and $m_{\alpha}^* = 0.16 m_0$ and $m_{\gamma}^* = 0.75 m_0$ for SnPd₃. Moreover, fitting the field dependence of the amplitude of the quantum oscillations yields $T_D(\alpha) = 25$ K with $\mu_{\alpha} = 713$ cm²V⁻¹S⁻¹, and $T_D(\gamma) = 42$ K with $\mu_{\gamma} = 134$ cm²V⁻¹S⁻¹ for PbPd₃ while $T_D(\alpha) = 53$ K with $\mu_{\alpha} = 252$ cm²V⁻¹S⁻¹, and $T_D(\gamma) = 10.6$ K with $\mu_{\gamma} = 270$ cm²V⁻¹S⁻¹ for SnPd₃.

Corroborated with the measured Seebeck coefficient, our Fermi surface mapping, through torque magnetometry measurements, reveals that E_F is about 54 meV and 68 meV above the flat bands for PbPd₃ and SnPd₃, respectively. E_F tuning is therefore essential in order to access the flat band to observe their contributions to the physical properties. The contributions of Pb and Pd orbitals to the band structure of PbPd₃ (Fig. S3) indicate that the flat band is mainly formed by the Pd 4*d* bands. Therefore, monovalent doping on the Pb/Sn site is expected to lower the E_F while maintaining the dispersion of the flat band. In order to study the surface state, on the other hand, E_F will need to be tuned away from the flat band (tune up in energy) to escape from the dominant bulk bands. For SnPd₃, although E_F is very close to the predicted surface state, the fact that the residual resistivity of SnPd₃ is higher than that of PbPd₃ (Fig. S1) suggests either the absence of topologically protected surface states in SnPd₃ or that the measured transport properties are completely dominated by the bulk state. To clarify this point, careful transport studies attempting to disentangle the contribution of the bulk state and that of the surface state of this material to its electrical conduction are required. Notice that the experimentally determined position of E_F for SnPd₃ implies that one should already have topological and linearly dispersing states on its surface (Fig. 4 (b)), making this compound ideal for such a study.

In summary, large single crystals of APd₃ ($A = \text{Pb, Sn}$) were grown by the Czochralski technique, and PbPd₃ was also grown by the molten flux method. The measured Seebeck coefficient suggests that the E_F is located above their flat bands. We further studied the geometry of the Fermi surfaces for both compounds through the dHvA effect. The topography of the Fermi surface revealed by the dHvA oscillations (under fields up to 45 T) suggest that the position of E_F for both compounds is at a higher energy than the values calculated by DFT, namely 54 meV higher for PbPd₃ and 68 meV higher for SnPd₃. As the flat-band feature is mainly contributed by the 4*d* bands of Pd, we propose that monovalent dopants on the Pb/Sn site will lower the E_F and

potentially provide access to the flat band. Furthermore, our experimental E_F suggests that in addition to the flat band in the bulk state, the Fermi arc and the Dirac surface states of SnPd_3 should be already accessible to the angle-resolved photoemission spectroscopy.

The data that support the findings of this study are available from the corresponding author upon a reasonable request.

ACKNOWLEDGMENTS

The National High Magnetic Field Laboratory is supported by National Science Foundation through NSF/DMR-1644779 and the State of Florida. KW acknowledges the support of the Jack E. Crow Postdoctoral Fellowship. KWC was partially supported by the NHMFL-UCGP program. JN acknowledges support from the National Science Foundation under award NSF/DMR-1606952, TS under award NSF/DMR-1534818, and GSN under award NSF/DMR-1748188. LB is supported by DOE-BES through award DE-SC0002613.

REFERENCES

- [1] K.-H. Ahn, W. E. Pickett, and K.-W. Lee, *Phys. Rev. B* 98, 035130 (2018).
- [2] N. P. Armitage, E. J. Mele, and A. Vishwanath, *Rev. Mod. Phys.* 90, 015001(2018).
- [3] B. Yan and C. Felser, *Annu. Rev. Condens. Matter Phys.* 8, 337 (2017).
- [4] Z. K. Liu, B. Zhou, Y. Zhang, Z. J. Wang, H. M. Weng, D. Prabhakaran, S.-K. Mo, Z. X. Shen, Z. Fang, X. Dai, Z. Hussain, and Y. L. Chen, *Science* 343, 864 (2014).
- [5] E. Tang and L. Fu, *Nature Phys.* 10, 964 (2014).
- [6] V. J. Kauppila, F. Aikebaier, and T. T. Heikkilä, *Phys. Rev. B* 93, 214505 (2016).
- [7] P. Ravindran, P. Vajeeston, R. Vidya, A. Kjekshus, and H. Fjellva, *Phys. Rev. B* 64, 224509 (2001).
- [8] K. Mori, H. Sakakibara, H. Usui, and K. Kuroki, *Phys. Rev. B* 88, 075141 (2013).
- [9] Z. Zhang and J. T. Yates, Jr., *Chem. Rev.* 112, 5520 (2012)
- [10] W. G. Zeier, J. Schmitt, G. Hautier, U. Aydemir, Z. M. Gibbs, C. Felser and G. J. Snyder, *Nature Rev. Mater.* 1, 16032 (2016).
- [11] N. J. Ghimire, Mojammel A. Khan, A. S. Botana, J. S. Jiang, and J. F. Mitchell, *Phys. Rev. M* 2, 081201(R) (2018).
- [12] J. Martin and G. S. Nolas, Apparatus for the measurement of electrical resistivity, *Rev. Sci. Instrum.* 87, 015105/1-8 (2016).
- [13] K. Schwarz, P. Blaha, and G. Madsen, *Comp. Phys. Comm.* 147, 1 (2002).
- [14] J. P. Perdew, K. Burke and M. Ernzerhof, *Phys. Rev. Lett.* 77, 3865 (1996).
- [15] P. M. C. Rourke and S. R. Julian, *Computer Physics Communications* 183, 324 (2012).
- [16] G. S. Nolas, J.W. Sharp and H. J. Goldsmid, *Thermoelectrics: Basics Principles and New Materials Developments*, Springer-Verlag, Berlin, 2001.
- [17] See Supplemental Material at [URL will be inserted by publisher] for other thermoelectric properties, low frequencies for the flux-grown PbPd₃, and the contributions of Pb and Pd orbitals to the band structure of PbPd₃.
- [18] D. Shoenberg, *Magnetic Oscillations in Metals*, Cambridge University Press, Cambridge, 2011.

Figures

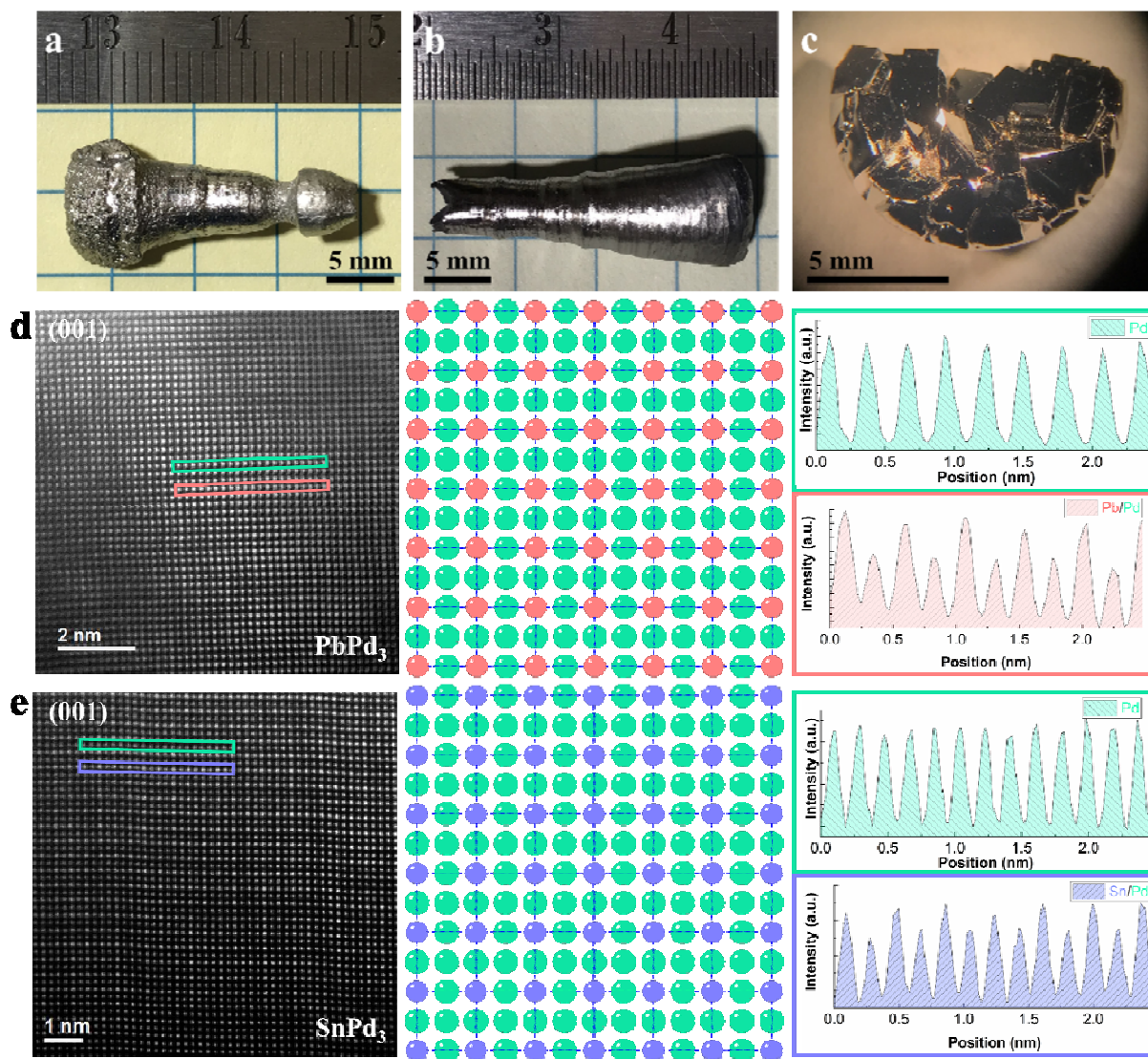


Figure 1. Pictures of Czochevski-grown crystals: (a) PbPd₃, (b) SnPd₃, and (c) flux grown PbPd₃. HAADF-STEM images of Czochevski-grown (d) PbPd₃ and (e) SnPd₃ are both shown in <001> projection with EDS line-scan included.

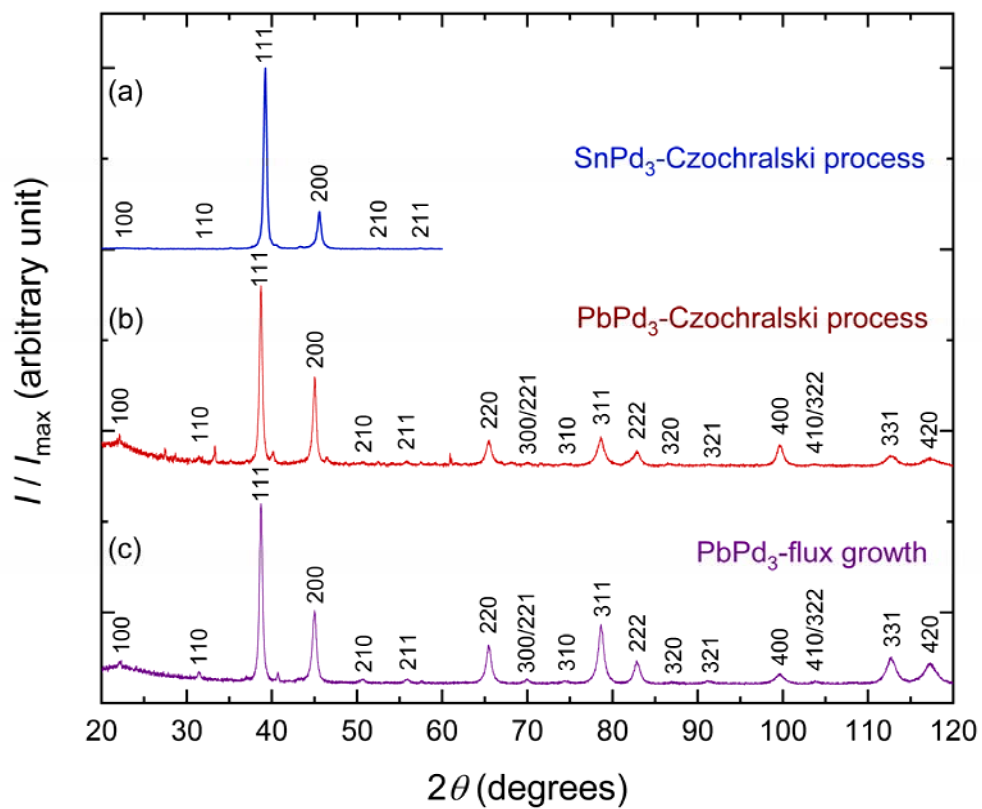


Figure 2. Indexed powder XRD patterns of (a) SnPd₃ and (b) PbPd₃ grown through the Czochralski process and (c) PbPd₃ grown through molten flux. (a) SnPd₃ pattern was acquired using a high signal/noise custom built X-ray system due to the weak superstructure intensities, (b) and (c) were collected using a Scintag PAD-V diffractometer.

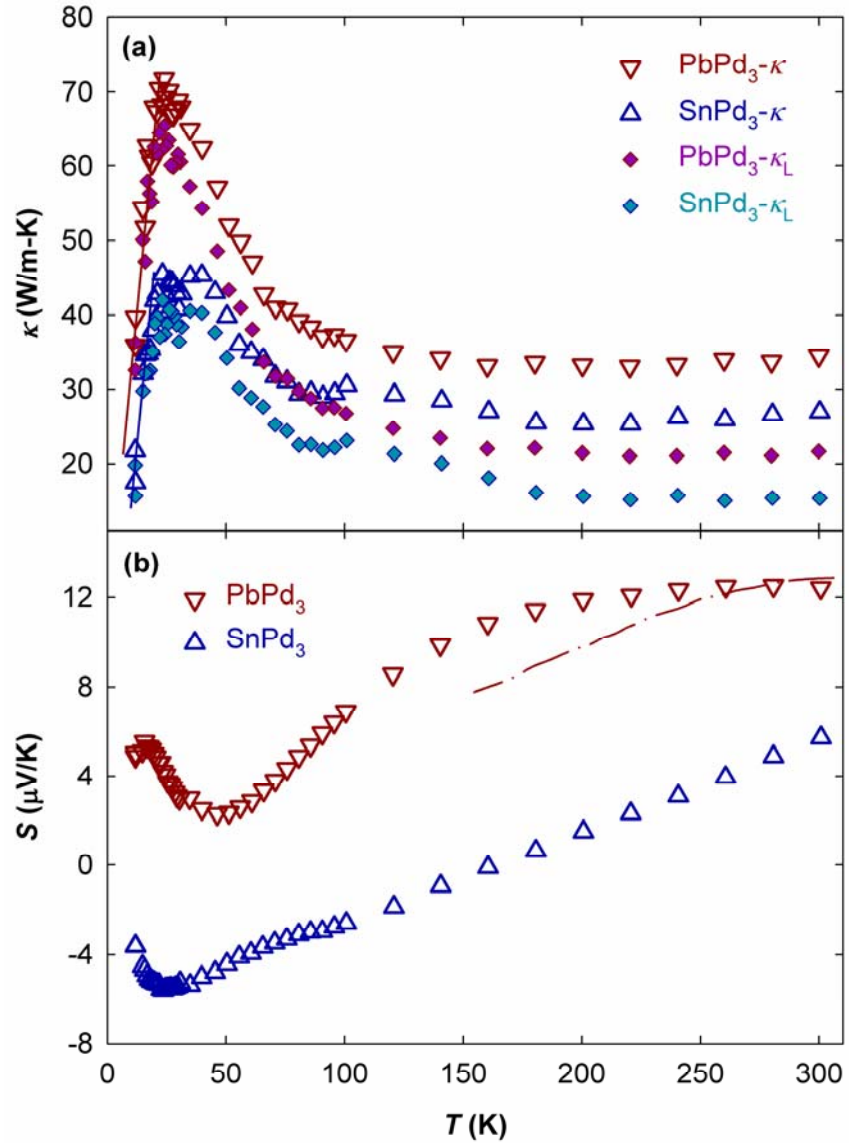


Figure 3. Temperature dependence of (a) the thermal conductivity κ and (b) the Seebeck coefficient S of PbPd₃ (dark red triangles) and SnPd₃ (dark blue triangles). The solid diamond-shape dots depict the lattice contribution to the thermal conductivity, κ_L , of PbPd₃ (violet diamonds) and SnPd₃ (blue diamonds). The solid lines in (a) represent the T^3 temperature dependence. The dash-dot line in (b) is the calculated temperature dependent Seebeck coefficient of Pb_{0.97}Bi_{0.03}Pd₃ from reference [1].

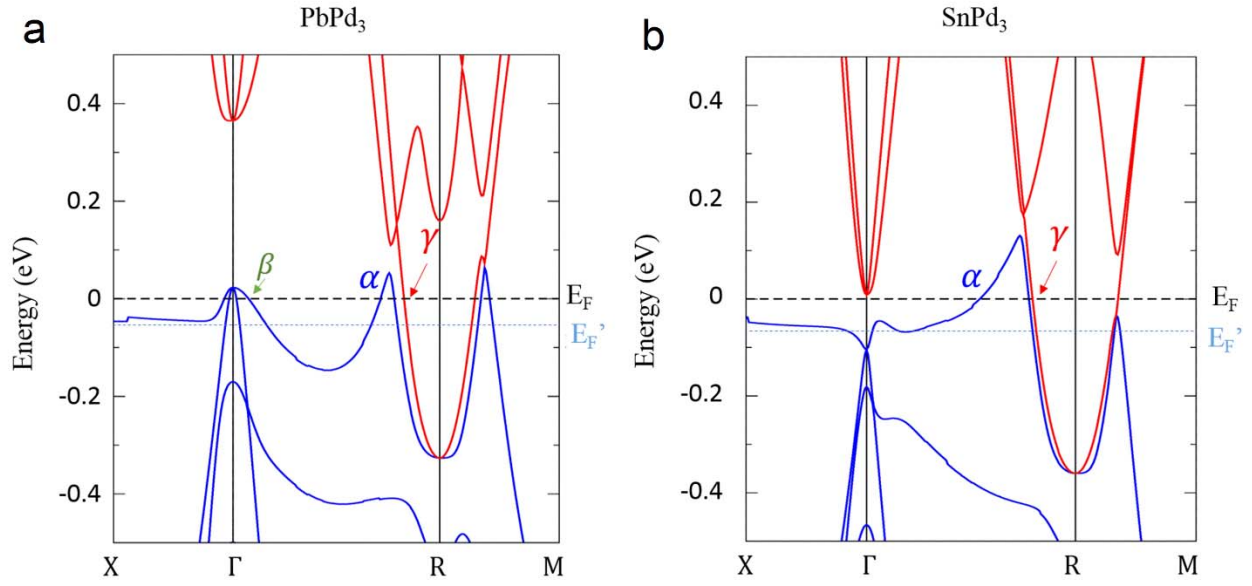


Figure 4. Calculated band structures of (a) PbPd_3 and (b) SnPd_3 . The Fermi level E_F' is the value directly obtained from the DFT calculations, which is consistent with reference [1]. E_F is the shifted Fermi level based on the experimental quantum oscillation data. $E_F - E_F' = 54$ meV for PbPd_3 and $E_F - E_F' = 68$ meV for SnPd_3 . Flat bands along the X - Γ lines and the Fermi surface cross-sectional areas associated with the α , β , γ dHvA orbits are indicated by arrows.

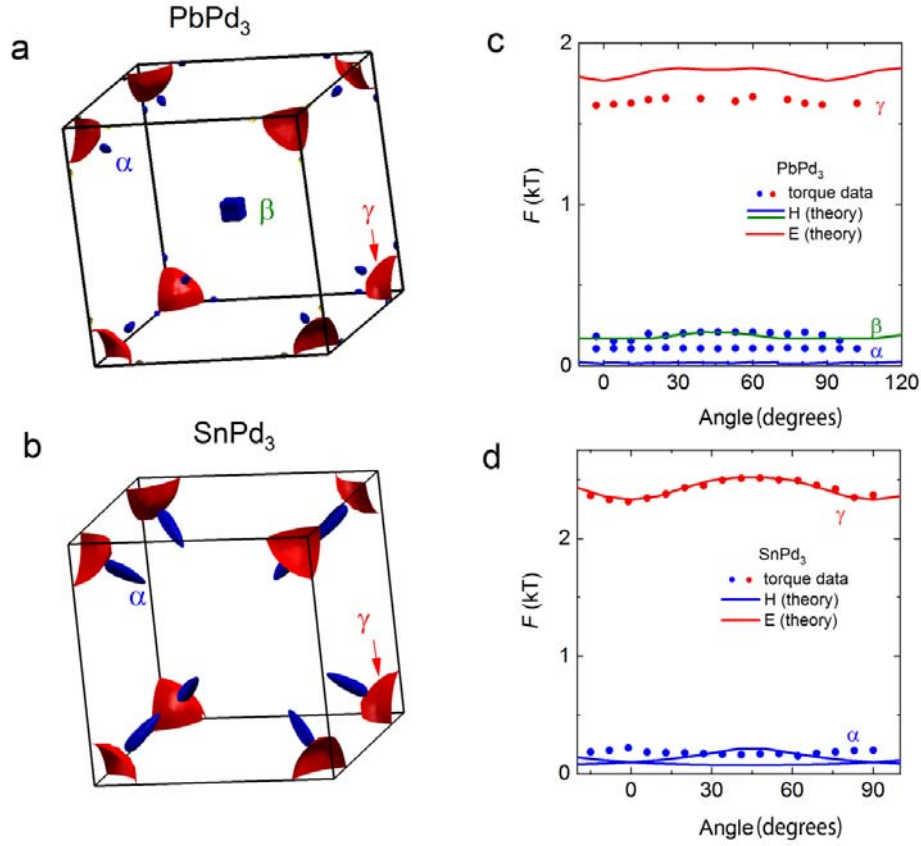


Figure 5. Fermi surfaces for the shifted Fermi level E_F : (a) PbPd_3 and (b) SnPd_3 . Hole- and electron-like pockets are depicted in blue and in red, respectively. The α orbit can be associated to an ellipsoidal hole pocket and the γ orbit to a large, nearly spherical electron pocket. The cubic β pocket near the Γ point only appears in PbPd_3 . (c) and (d) show the Cyclotron frequencies F as a function of the angle θ relative to the crystallographic $[001]$ -axis.

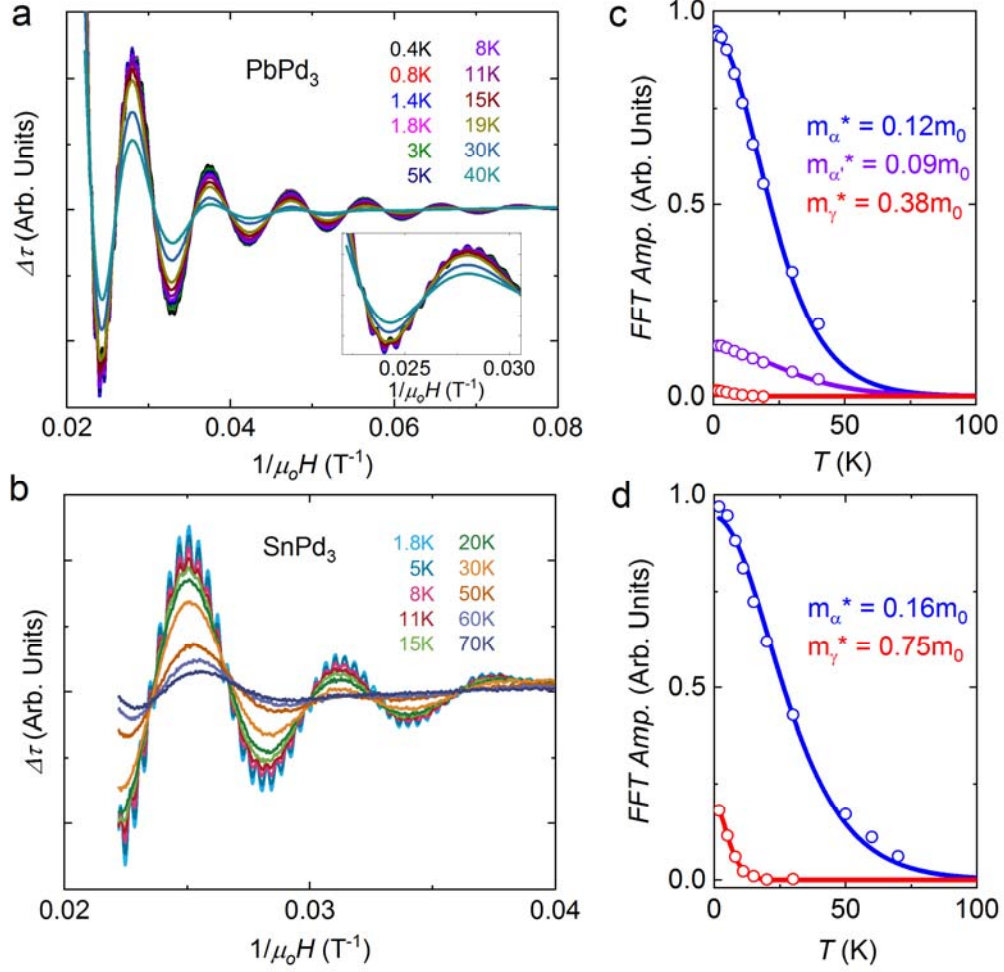


Figure 6. (a) Background subtracted torque $\Delta\tau$ for PbPd_3 showing dHvA oscillations at $\theta = 14^\circ$ and at various temperatures. Inset: dHvA signal in a limited magnetic field range, i.e. $\mu_0H = 30 - 45$ T. (b) $\Delta\tau$ for SnPd_3 at $\theta = 14^\circ$ at various temperatures. Amplitude of the main peaks observed in the Fast Fourier transforms (FFT) spectra of the dHvA signal as a function of temperature are shown for (c) PbPd_3 and (d) SnPd_3 , respectively. Solid lines are fits to the Lifshitz-Kosevich formula [18] yielding the carrier effective masses.